FFEMS Fatigue & Fracture of Engineering Materials & Structures
ORIGINAL CONTRIBUTION
doi: 10.1111/ffe.12360

Evaluation of environmentally assisted fracture of austempered ductile iron (ADI) under cyclic load bearing

F. FERNÁNDEZ SCUDELLER and R. A. MARTÍNEZ

División Metalurgia, INTEMA–UNMDP–CONICET, Mar del Plata, Pcia. de Buenos Aires República Argentina

Received Date: 16 April 2015; Accepted Date: 6 September 2015; Published Online: 2015

ABSTRACT This paper aims to characterize the behaviour of austempered ductile iron (ADI) under cyclic load bearing and its surface in contact with water.
The first part is devoted to verifying the drop in Ultimate tensile strength and the elongation that takes place when ADI tensile samples are tested submerged in water as compared to values obtained in dry condition.
Focus of this work is placed on crack initiation and propagation when submerged SEN (B) samples are tested applying cyclic loads.
Different test stages of fissure nucleation and propagation on the lateral face of the sample were documented by microscopic imaging during the test, thereby allowing to characterize the manner in which failure occurred.
The resulting fracture surfaces were analysed by scanning electron microscopy (SEM), and possible fracture mechanisms are discussed.
The main contributions of this work include characteristic values of the time of crack initiation, crack growth rate and a methodology to study some particularities of the operating fracture mechanisms based on lateral observations and fracture surface images.

Keywords ADI; cracks; cyclic load; embrittlement; water.

NOMENCLATURE

tn = Nucleation time
te = specific nucleation time
Sr = ligament surface
Vc = growing rate

INTRODUCTION

Spheroidal graphite cast iron reaches very high strength when an austempering heat treatment is conducted. The resulting matrix features a microstructure composed by a combination of acicular ferrite and high carbon austenite, frequently referred to as 'ausferrite', typical of the material called austempered ductile iron or simply ADI.

ADI can be produced in different strength grades depending on the temperature through the isothermal part of the heat treatment, reaching properties ranging from 850 MPa to 1600 MPa of tensile strength, and elongation between 10 and 0 respectively.[1]

The outstanding mechanical properties of ADI, in conjunction with its low cost, allow to obtain cast parts very close to their final operative shape, turning this material into a natural substitute for cast or forged steel and making it widely used for the fabrication of parts for different industries such as rail road, automotive and agricultural, to name a few.

However, the mechanical behaviour of ADI suffers a curious embrittlement phenomenon when tested with its surface in contact with liquids, mainly water.

This degradation singularity has been reported by Komatsu *et al.*[2,3] and by Martínez *et al.*[4–6] The effect of water on mechanical properties is independent of its pH, when water based solutions of pH ranging from 5.5 to 11.9 are used.[4]

The phenomenon has been characterized using different assessment methods including mechanical, electrochemical and metallurgical, among others. A brief review of the knowledge existing at the present time is cited is briefly as follows:

- Based on the results of tensile tests on cylindrical samples, drops in Ultimate tensile strength of around 15–20% and

Correspondence: R. A. Martínez. E-mail: rimarti@fi.mdp.edu.ar

a 75% fall in elongation were verified, while the 0.2% offset strength remained at the same level.[4–6]
- When testing the fracture toughness of the material, values of k_{IC} measured in submerged samples dropped nearly 50% as compared to the results obtained in dry conditions.[7]
- When testing samples submerged in different liquids, it was shown that water causes the most deleterious effect in terms of mechanical properties degradation, while other fluids, such as alcohol and organic substances, result in different degrees of embrittlement.[8]
- Hydrogen embrittlement (HE) involves brittle fracture caused by penetration and diffusion of atomic H into the crystal structure of an alloy.

When ADI was tested applying a controlled electrochemical potential in order to favour or inhibit proton generation on the sample surface, the differences observed were not significant. This fact studied by Masud *et al.*[9] and Caballero *et al.*[10] led to conclude that the phenomenon is not of the 'hydrogen-induced embrittlement' type.

- HE, together with stress corrosion cracking (SCC) and liquid metal embrittlement (LME) are the most extensively studied environmentally assisted fracture (EAF) processes.[11–13] Corrosion rates are usually quite low when compared with the very fast process developed by ADI in water. The phenomenon under study in this work present similitude with LME, which causes the catastrophic brittle failure of normally ductile metal alloys when coated by liquid metal and stressed in tension.[14] In most cases, the initiation and the propagation of cracks appear to occur instantaneously, with the fracture propagating through the entire test specimen. The velocity of crack or fracture propagation has been estimated to be 10 to 100 cm s^{-1}[19]

It was verified that the embrittlement of ADI with water occurs instantaneously, i.e. is independent of the period of time in which the sample surface is wet. A good example of this statement is illustrated by a particular test. If a sample tested in dry conditions is loaded at a level lower than that for dry fracture although higher than that for wet failure (plastic zone) and touched in the calibrated section with a wet cotton swab, it immediately collapses, supporting the fact that the presence of water in the surface of a strained sample (with microcracks) is enough to start the rapid fracture process.[15]

Another issue worth mentioning is that after a submerged sample is dried and tested, the embrittlement phenomenon does not occur.

Indeed the failure process starts in a superficial crack that allows water to penetrate and weaken the crack tip producing growth at a very fast rate.[16]

Probably, for a better understanding of this phenomenon, ductile iron microstructure should be addressed in the first place. The resulting characteristic microstructure of ADI is directly related to the solidification process of the base ductile iron. A brief description of this process could start with graphite and austenite nucleation in the liquid, with austenite growing dendritically. As the solidification event advances, the austenite dendrites trap the surrounding nodules, and then the dendrites and nodules grow together into isolated liquid zones that solidify at the end of the process. The resulting zones between dendrites are known as 'cell boundaries' or as last to freeze (LTF) regions.[17]

Given the fact that LTF zones solidify at the end of the process, the concentration of some alloy elements may diffuse and concentrate in these zones as well as in porosity and shrinkage cavities.[17]

As a consequence, microsegregation (macrosegregation can be 'controlled' in the same way) promotes microstructural differences in the bulk zones of the metallic matrix.[18]

It is evident that the size and distribution of the LTF zones define the material quality and play a key role in this process called EAF of ADI. Given the myriad of hard and fragile components present in LTFs, they act as a crack source when the sample is at the early stages of plastic deformation[19,20] (Fig. 1).

The goal of this work is to explore and characterize this particular phenomenon when load bearing is of cyclic nature, in order to expand the knowledge of EAF on ADI, specifically on the mechanical properties affected.

EXPERIMENTAL PROCEDURE

The material used in this work was obtained by pouring a melt on 25 mm Y-block molds (ASTM A 536-84) and following conventional practices of nodulization, inoculation

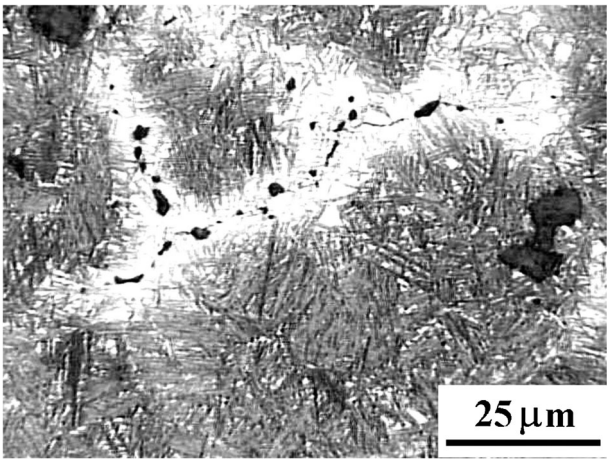

Fig. 1 Crack developed in LTF at first stages of plastic deformation.

and cast at the experimental casting laboratory of the Metallurgy Division at the INTEMA.

The chemical composition was determined by using an optical spark emission spectrometer BAIRD DV6.

From the Y blocks obtained, rectangular prisms of $12 \times 25 \times 100$ mm and cylindrical bars of 12 mm diameter were cut and mechanized to obtain SEN(B) (ASTM E399-90) and tensile (ASTM E8M/88/04) specimens, respectively.

Prior to the final machining process, an austempering heat treatment was conducted using an austenitizing temperature of 910 °C for 1 h. Afterwards, the samples were submerged in a salt bath at 360 °C for 1 h and a half.

The final size and shape of the specimens used are provided in Fig. 2.

The machined notch of the SEN (B) samples was 10 mm length and 1.5 mm width, with an angle of 45°.

Tensile tests were carried out using a Mohr and Federhaff 40 ton maximum capacity Universal Testing Machine. The 0.2% offset strain was measured with an MTS model 432.11 F-20 extensometer.

The cyclic load test was performed by using a mechanical testing machine with a double-eccentric actuator applying a displacement-controlled cyclic load. A maximum load of 2.2 kN approximately was applied using a constant eccentricity of $e = 0.145$ mm. A stress ratio $R = 0$ was chosen for all tests. This resulted in stable crack propagation under small-scale plasticity conditions. Under these conditions, the crack plastic zone extent, r_p, never exceeded 1% of the crack length, which is in accordance with the procedures reported in the literature.[21] The frequency of the cyclic load applied was 6 Hz.

The setup used to carry on the tensile and cyclic load bearing tests in wet conditions is shown in Fig. 3. Tap water with ph7 was used, and the tests were carried out at room temperature of the lab (20 °C)

The lateral surfaces of SEN(B) samples were prepared using conventional methods for grinding and polishing. Nital (2%) was used as etchant, and samples were observed under light microscopy. Before running the tests, a band made up of several fields of the lateral faces was documented. This back-up allowed to compare the microstructure once the crack had passed and, in this way, to identify the microstructural region involved in the fracture process.

The experimental methodology used to measure lateral initiation and crack growth consisted in: (a) stopping the test periodically, (b) performing optical microscopic observations and (c) documenting crack propagation length and path by means of micrographs. Stops for observation were at regular 5 min periods.

All metallographic observations were conducted using an Olympus PGM3 microscope and fracture surfaces were examined under a JEOL JSM-6460LV scanning electron microscope.

In all cases, the reported results correspond to the average of at least three tests.

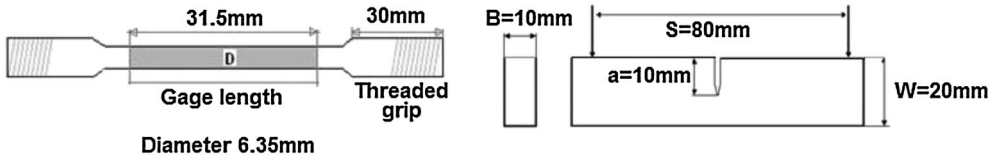

Fig. 2 Samples used for evaluation of mechanical properties.

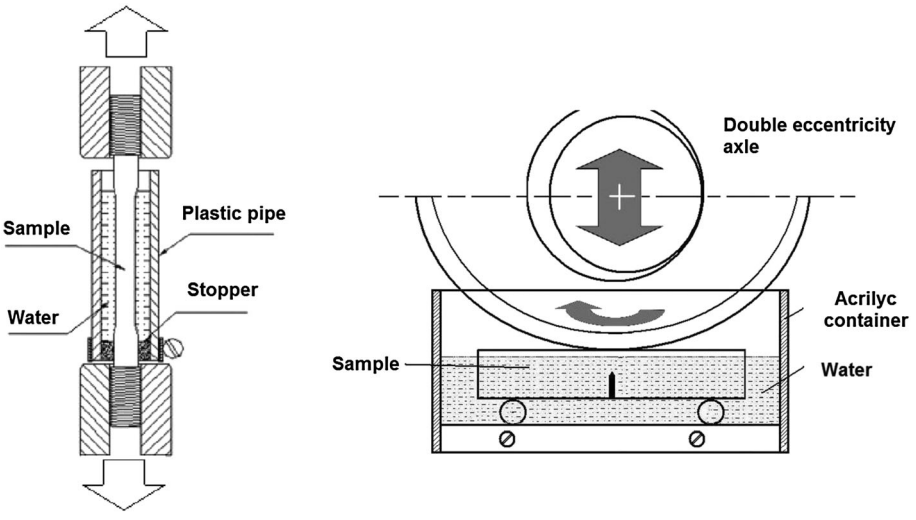

Fig. 3 Experimental setup used for tensile and cyclic load application.

RESULTS AND DISCUSSION

Table 1 provides the chemical composition of the melt used. The average nodular count was of 125 nod mm^{-2} with a nodularity of 90% and nodules size 8 according to ASTM A-247 standard (Fig. 4).

Tensile tests

The results obtained from the tensile test are summarized in Table 2. It is worth noticing that a 17.3% decrease in ultimate tensile strength and a 76.2% fall in elongation took place, although the 0.2% offset strain strength remained unaffected.

The results of this test confirm values reported in the literature[2,4] accounting for a substantial fall of elongation and a minor fall in ultimate tensile strength when tests are conducted on a submerged sample.

The failure of the submerged samples exhibited some degree of plastic deformation. The fracture mechanisms that govern embrittlement involve the cracks generated at the initial stages of plastic deformation in the LTF zones. Inside these micro cracks, the penetrating water generates a local chemisorption process that weakens the atoms located in the crack tip and lead to fast crack propagation.

Table 1 Chemical composition

C	Si	Cu	Ni	Mg	Mn	P	CE
3.58	1.95	1.08	0.38	0.046	0.18	0.02	4.23

CE, equivalent carbon.

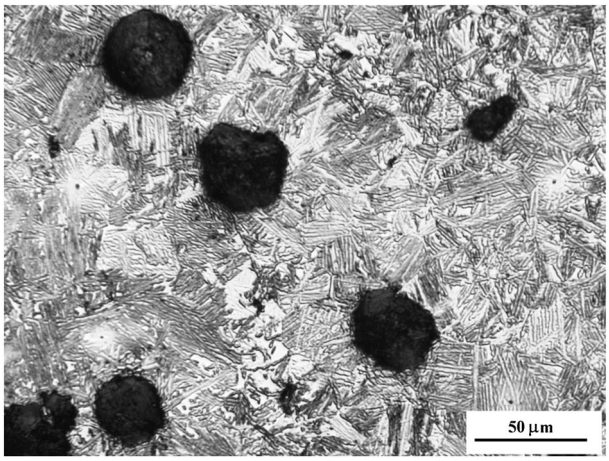

Fig. 4 Microstructure of the ADI used in this work.

Table 2 Tensile test properties

Property	Dry	Wet
Ultimate tensile strength (MPa)	1164.3	963.0
0.2% off set strength (MPa)	925.9	922.8
Elongation (%)	13.20	3.14

Cyclic loads

Crack behaviour on the lateral surfaces analysed, tested applying cyclic loads, is displayed in Fig. 5. The crack length is plotted against a number of cycles (or test time). As it can be noticed, submerged samples nucleate observable cracks earlier than those tested in dry condition, probably generated by the interaction of water with some defects on the surface that favours earlier nucleation.

With the purpose of avoid errors in crack rate estimation, it was verified that the front of the advancing crack (by observing a partially cracked and broken by overload sample) was very straight and did not hide the size of the crack measured at the lateral faces of the sample (Fig. 6).

Again, considering that LTF zones yield the highest density of defects in the material, in general terms, these zones are identified as the most probable sites for nucleation of the initial cracks with a preponderant role in the embrittlement process under study.

This result could be related with previous outcomes obtained from the analysis of the lateral surfaces of tensile samples[16], in which it was determined that the threshold stress for crack nucleation takes place at lower load values when the sample is tested in water.

Figure 5 also demonstrates that the crack growth rate is higher in the submerged sample test, a fact noticed by the steeper slope of the curve.

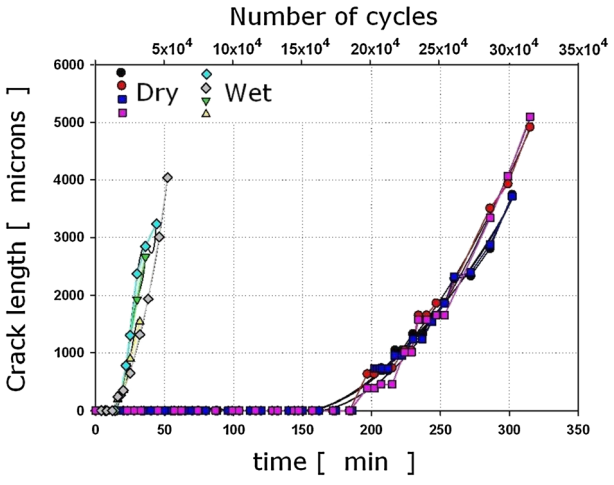

Fig. 5 Crack behaviour on the lateral surfaces of SEN (B) samples, tested applying cyclic loads.

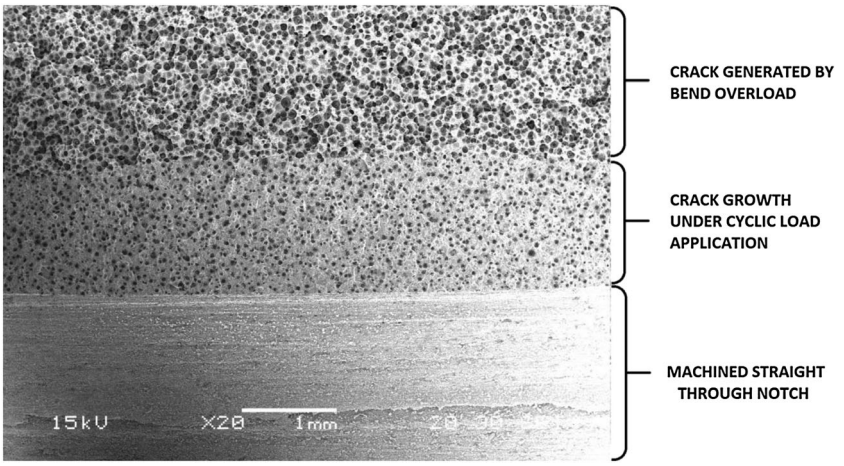

Fig. 6 Fracture surface of SEN(B) sample showing the machined notch, cyclic load growth crack and overload zones.

Table 3 lists the average values of nucleation time (t_N) when considering several lateral surfaces of the samples. Nucleation time represents the time elapsed from the start of load application to the moment of the first crack seen under the optical microscope (cracks of around 8–10 microns). This same table also provides the calculated growing rate (V_C). Finally, a calculated parameter, called specific nucleation time, t_E, is reported. This parameter is defined as the ratio of the observed time relative to the ligament surface at the beginning of the test, which is measured in the fragmented pieces after the break.

The reason to introduce this parameter could be understood in the basis of the independence of the sample size, given the fact that the machined crack can be different from sample to sample.

Table 3 Cyclic load application average results

Test condition	t_N [min]	$t_E = t_N/Sr$ [min mm^{-2}]	V_C [μm min^{-1}]	Cycles
Dry	192	1.74	32.1	1.97×10^5
Wet	21	0.16	112.3	6.9×10^5

The measured values of nucleation and growth of cracks were repetitive, the difference among stops never exceed ±4% of difference in length.

It is possible to confirm that the application of cyclic loads under wet conditions severely affects both crack nucleation and crack growth in ADI.

These two results (earlier crack nucleation and higher crack growth rate) extend existing knowledge about the failure process of ADI when its surface is in contact with water. The presence of water in the surface of a sample working under cyclic loads produces the generation of cracks earlier than a sample operating in dry conditions.

Once a crack is generated in the surface of the material, it will grow faster when water penetrates inside it compared to the growing rate without the fluid in the crack tip.

Figure 7 places the new advance obtained in this work with the existing knowledge including the embrittlement effect of water at a low load application rate (tensile and three-point-bending tests)[3,4,7] and not evident at high speed load applications (impact test).[4]

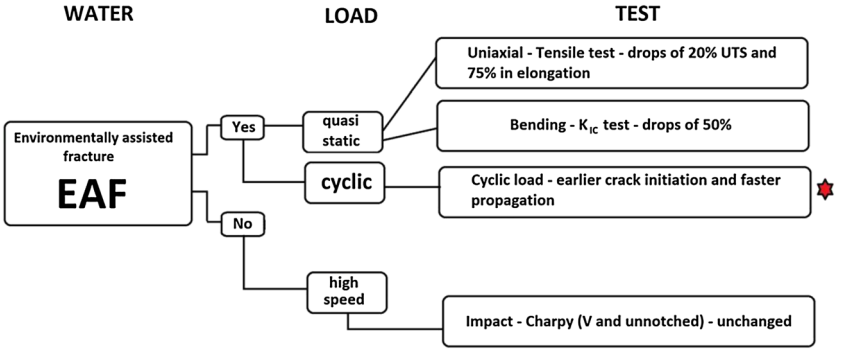

Fig. 7 Mechanical properties of ADI evaluated in aqueous environment. State of the art.

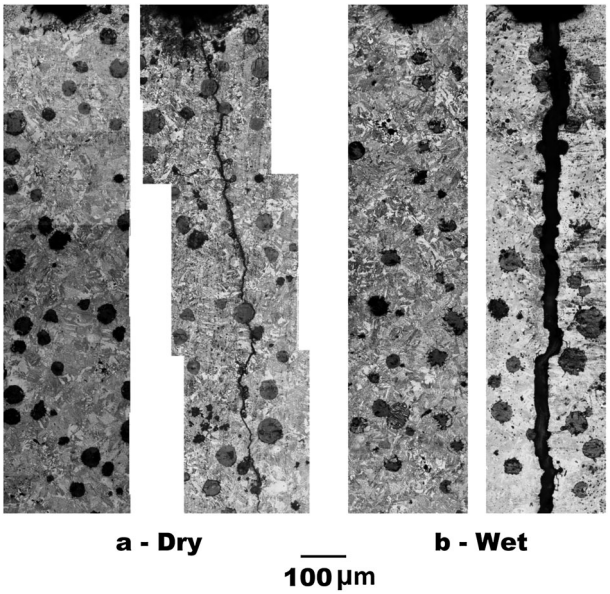

Fig. 8 Crack propagation zone on lateral surface of the sample in dry (a) and wet (b) conditions.

STUDY OF CRACK PROPAGATION ON LATERAL SURFACES

Figure 8 illustrates the zone where the crack propagates in dry (a) and wet (b) conditions. Both figures illustrate the zone before and after propagation. By following the propagation line, it is possible to identify microstructural sectors that are more likely to play a part in the fracture process.

The crack in the dry tested samples grew following a zigzag path, while in the wet specimens the course followed a more straight line. In the first case, the propagating crack followed the line determined by the ausferrite matrix needles, whereas in the second one such direction was only followed if the needles were aligned, otherwise the advancing crack cut the needles bunches (Fig. 9). This could explain the change in the slope of the crack growing curve because a more intricate path takes longer than a straight one does.

The cracks in the samples tested in air have shown a path more likely to connect neighbouring nodules. In submerged tested samples, this is not as rigorous.

Both dry and submerged cracks chose LTF zones as their preferential path when they spread near said zone. This is a logical behaviour considering that these zones presented higher degree of segregation and casting defects such as pores, inclusions and carbides as it was previously mentioned.

It is also worthy to mention that the nodular cavities passed by dry crack featured higher strain than those tested in water.

In order to measure the nucleation process and crack progress, observations were carried out in samples not etched so as to better observe the fissure. As an example, Fig. 10 displays a sample tested dry with clear signs of plastic deformation both in the fissure and in the surrounding area. Conversely, in submerged samples, the macro appearance did not show lateral contraction signals, thereby indicating that strains associated with environmentally induced brittle fractures were smaller and more localized than those associated with ductile fracture.

Fracture surfaces

Uniaxial load application

Figure 11 reveals the fracture surface of a tensile sample tested in dry conditions with enlarged nodular cavities and metallic matrix areas (lips displayed as white lines) with evident signs of plastic deformation. A combination of fracture mechanisms seems to have occurred; also dimples can be distinguished in these areas between the nodules. The process begins with micro void nucleation and second phase particle growth, such as those present in LTF zones (Fig. 12). Probably, cleavage zones generated when the propagating crack advanced in the LTF zones

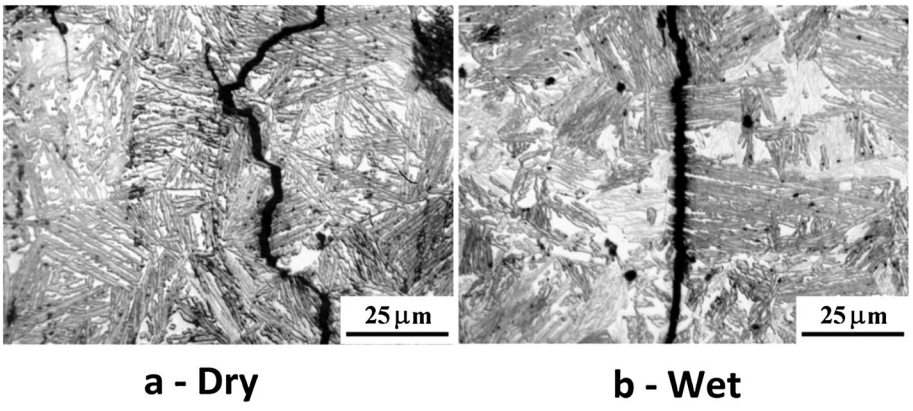

Fig. 9 Characteristics of propagation in dry (a) and wet (b) conditions.

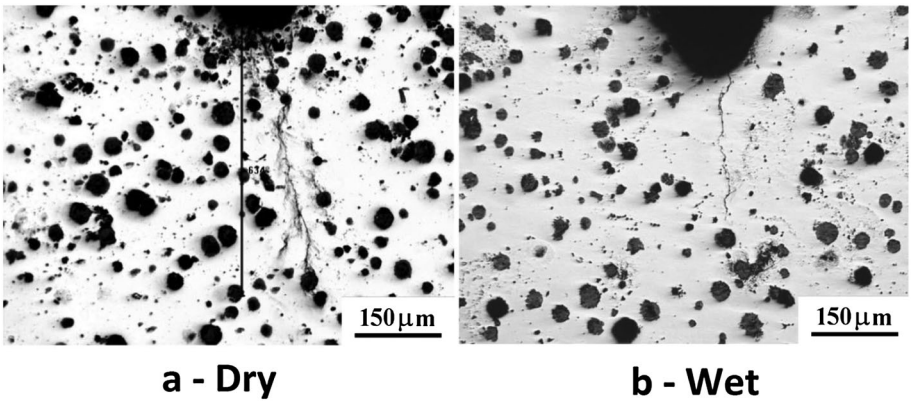

Fig. 10 Difference in plastic deformations signs in crack nucleation (a—dry, b—wet).

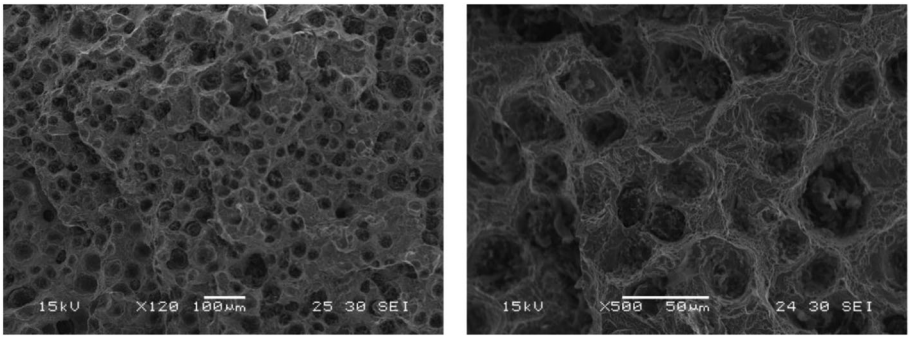

Fig. 11 Fracture surface of tensile sample tested in dry condition.

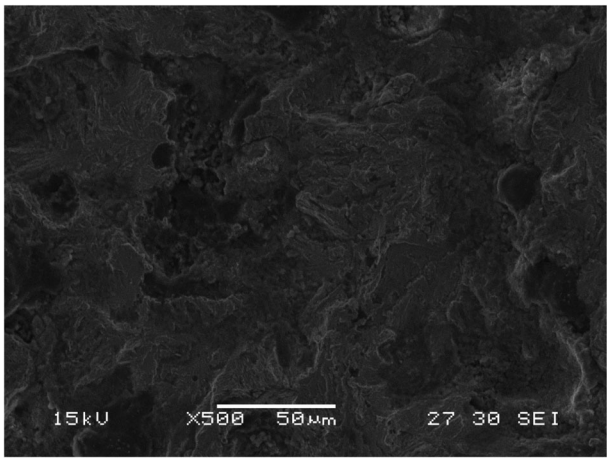

Fig. 12 LTF zone.

as ductility properties are lower than those of ausferrite. This mode of fracture is often called *quasi-cleavage*.[22]

The quasi-cleavage mechanism can be understood by analysing the initiation of small cracks ahead of the main crack front, especially in some preferentially oriented planes, that cleave. First, these small cracks grow in a brittle manner that later becomes ductile striation, finally joining the main crack front. The main mechanism is given by small cracks emanating from nodules and LTF zones growing towards the main crack. In other words, the propagation of the main crack is partly explained by the initiation and backward growth of small cracks that initiate from certain irregularities in the material.[22]

It should be taken into account that several nodules can be involved in the growth process at different portions of the crack front, so growth rate is affected by the size, shape and distribution of graphite nodules as well as by the size and distribution of LTF zones.

Figure 13 (a) illustrates the fracture surface of a tensile specimen with its gage length totally submerged in water. Two very different areas can be observed. The figure shows a shiny and flat area (marked) which has been also identified in previous papers as the site where the fracture originates.[1,4]

This zone exhibits a particular propagation mechanism with a fully cleavage flat aspect, as shown in detail in Fig. 13 (b). The appearance of the remaining surface is similar to that described in the paragraph above for the tensile test conducted in air where the quasi-cleavage

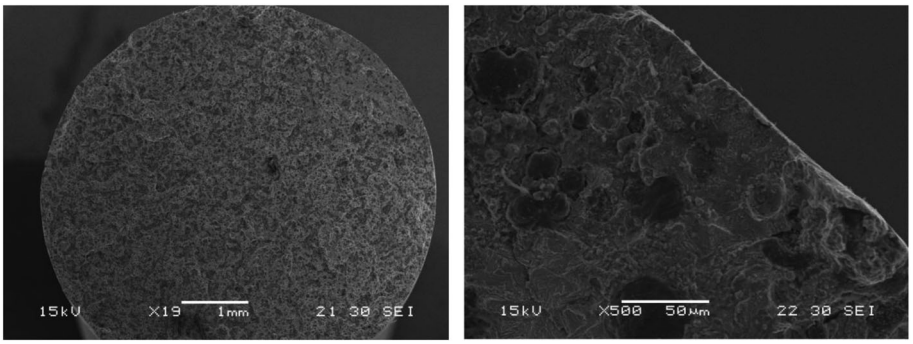

Fig. 13 Fracture surface of tensile sample tested in wet condition.

mechanism acted. This means that the fracture initially started with a low energy consumption mechanism and then shifted to an increased energy consumption mechanism.

Cleavage involves breaking bonds; local stress must be sufficient to overcome the material cohesive strength. The susceptibility to start a cleavage fracture is enhanced by almost any factor that increases yield strength, such as water penetration into the surface defect in the material.

Different causes could be responsible for this mode of total fracture, for example, the crack is arrested at the nodule–matrix interface. The nodule breaks because of the strain in the matrix, yet the crack cannot propagate because the local stress applied is less than the required fracture stress. This crack does not reinitiate because subsequent deformation and dislocation motion in the matrix cause the crack to blunt.

However when the size of the cleavage zone generated during the initial stage exceeded the critical size (about 0.8 mm), the remaining ligament was unable to withstand the applied load and overload failure occurred with the quasi cleavage mechanism.

Cyclic load application

Figure 14 (a), which illustrates a dry test with applied cyclic loads, shows a fracture surface very different from that observed in tensile specimens. A low magnification flat surface reveals areas with angular white lines or 'lips'; the fracture is characterized by deformation or stretch marks in different facets, sizes and micro morphologies. Groove orientation seems to be related to the forward direction, showing changes in orientation as they approach the nodules.

Certain plastic deformation could be noticed around the nodule holes, although to a lesser extent than that observed in the tensile test fracture surfaces. The fracture surface also shows a lower density of these holes. This would suggest that graphite does not play such a key part in crack propagation when cyclic loads are applied.[23,24]

Figure 14 (b) depicts the fracture surfaces of water immersed specimens subjected to cyclic loading where more cleavage facets can be distinguished. Wrinkles can also be observed, probably resulting from the behaviour seen in Fig. 10, as well as 'lips' of greater length and more rounded 'macrotongues' (compared to 14a). These nodules' density is even lower than that reported for dry conditions, suggesting that in submerged samples, cracks do not grow directly toward the nodules but rather propagate through the metal matrix, which seems to confirm the observations reported when the side faces of the samples were analysed.

The inhibited plastic deformation is attributed to the water penetration into the micro cracks originated in the sample surface, mainly at LTF zones and free places at strained nodular cavities or nodule–matrix interfaces.

However, slips occurred on planes intersecting crack fronts; strains just under fracture surfaces were substantial and small, not so deep dimples were generally observed on fracture surfaces associated to EAF. On the other hand, larger and deep dimples with small indentations inside were usually noticed on fracture surfaces generated in the ductile mode. It can be concluded that, in the presence of water, the mechanism occurs by a more localized process of microvoid coalescence than that in dry condition.

It is clear that the essential causes of EAF cracking are very difficult to find because crack-tip processes at the atomic level cannot be observed directly in the specimens under test. However, mechanisms of cracking can often be inferred from observations made on metallographic and fractographic techniques.

In agreement with Lynch research[25], the occurrence of a more localized process of plastic flow – microvoid coalescence when, for instance, an adsorbed metal (LME), or in our case water atoms are present at crack tips must be because of an effect of adsorption on the dislocation activity. The range of influence of adsorption is only several atomic distances for metals and hence adsorption can only affect the nucleation of dislocations at crack tips.

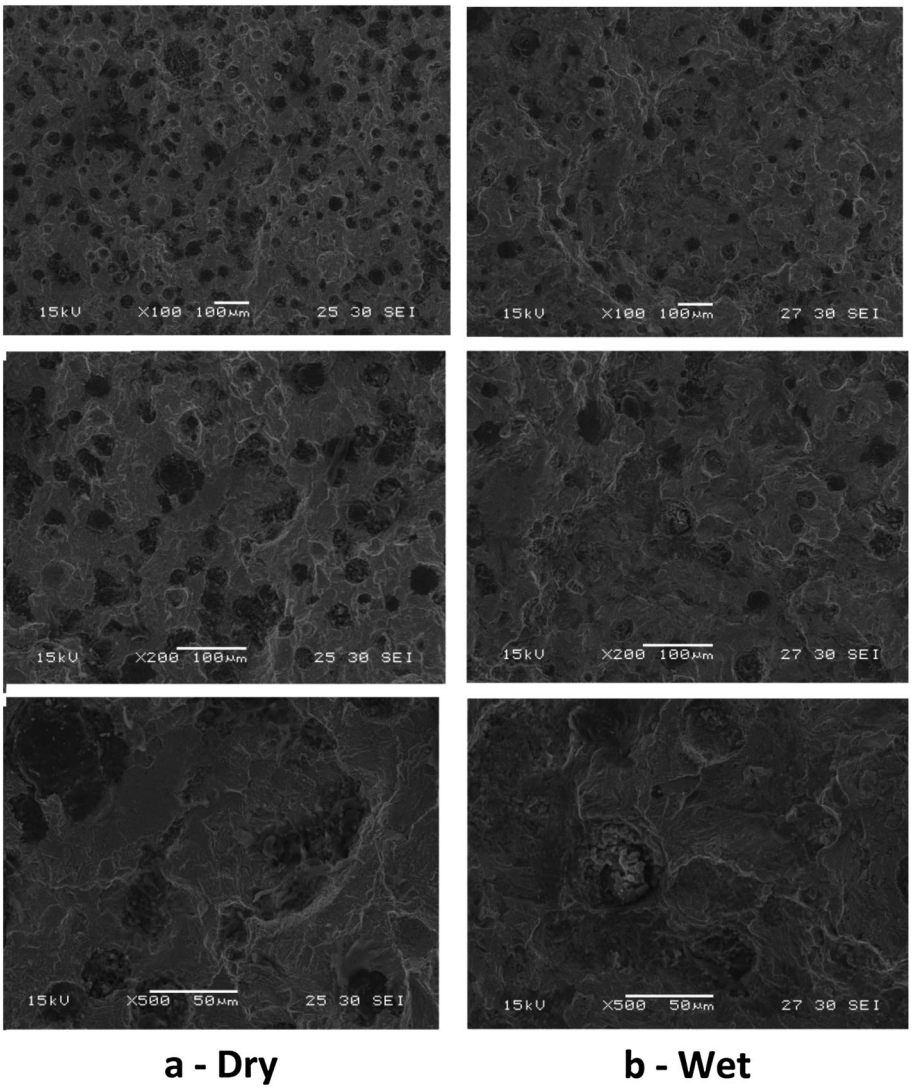

Fig. 14 Fracture surface of samples tested under cyclic load bearing (a: dry, b: wet).

Such a localized effect can explain the experimental observations made in dry and wet conditions in the following manner: ductile behaviour in dry conditions could be explained by the fact that numerous dislocation sources ahead of crack tips are activated at a lower stress than that required for dislocation nucleation at crack tips. Only a few dislocations nucleated at sources ahead of the crack tip egress, more precisely at crack tips, to produce crack advance (and opening) (Fig. 15a). Thus crack-opening displacements are largely lodged by blunting of the crack tip and by the development of large strains ahead of cracks. These strains result in void nucleation (or separation of nodule matrix interfaces) depending on the size, shape and type of particle.

Such role is played by widely spaced large particles (nodules) and by smaller particles between them (different shape and size into LTF zones). The coalescence of these large voids with crack tips involves the formation of smaller voids around smaller particles so that small dimples between and within large deep dimples are produced on the fracture surfaces (Fig. 15b).

The occurrence of a more localized microvoid coalescence process in aqueous environments is assumed on the basis that adsorption weakens interatomic bonds at crack tips, thereby facilitating the nucleation of dislocations from the crack tip so that sources in this zone are activated before extensive dislocation activity occurs ahead of cracks. Dislocations injected from crack tips on the appropriate inclined slip planes generate the crack advance and opening. Therefore crack opening displacement is accommodated by crack growth (Fig. 16a).

Smaller strains and smaller plastic zones will obviously be developed when crack growth prevails over crack blunting. Consequently large second phase particles

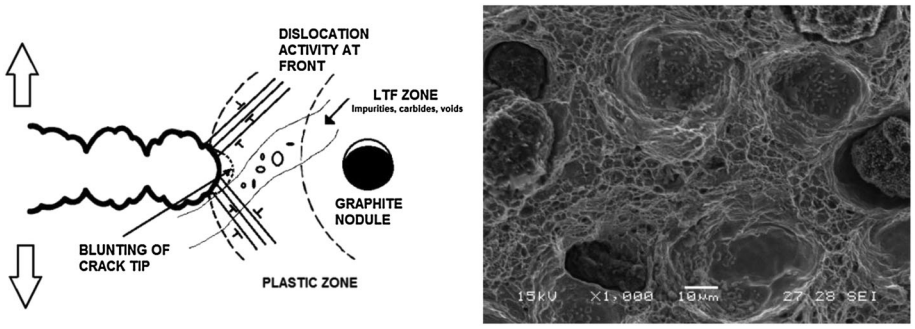

Fig. 15 Proposed ductile growth mechanism. Dry.

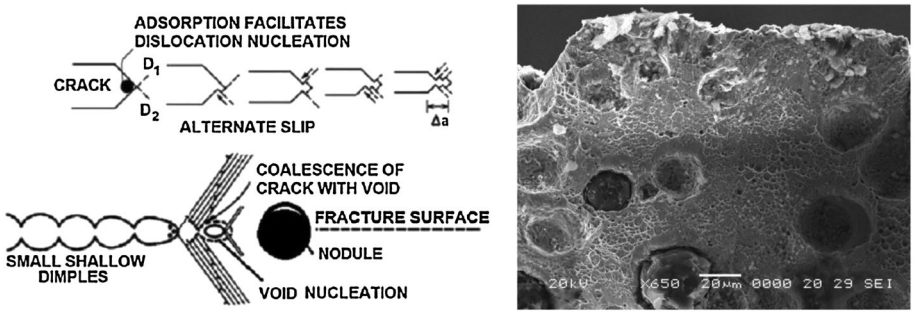

Fig. 16 Proposed brittle growth mechanism. Wet.

ahead of cracks are not developed by the plastic zone until they are close to the crack tip. Void growth around larger particles does not occur to the same extent as it does during ductile crack growth. Then the resultant fracture surface is mainly composed by small hollow dimples in brittle fracture surfaces (Fig. 16b).

CONCLUSIONS

- The application of cyclic loads to ADI samples immersed in water leads to a degradation of material properties. This statement allows to extend existing knowledge on the embrittlement phenomenon of ADI tested in water environment.
- Testing ADI submerged in water and applying cyclic loads affect directly crack nucleation and accelerate crack advance.
- Monitoring of crack advance in the side face of the specimens showed winding roads, a tendency to follow a path connecting nodules and signs of increased plastic deformation at the tip of the crack and nodular cavities when the specimens are tested dry. In turn, when tests are carried out with water, the propagation path is straight and with little plastic deformation.
- Fracture surfaces in dry conditions showed grooves and facets in different positions and different micro morphologies. Wet fractures featured a higher number of facets, rounded lip in the forward direction and a greater number of zones, which justifies the cleavage fracture mechanism with lower energy consumption and promotes the embrittlement phenomenon.
- Ductile and brittle behaviours under cyclic loads have been discussed in terms of dislocation activity in the neighbourhood of the crack tip.

REFERENCES

1 ASTM A 897 M-06. (1995) Standard specification for austempered ductile iron castings, *Annual Book of ASTM Standards*, ASTM International, Philadelphia.
2 Komatsu, S., Zhou C. Q., Shibutani, S. and Tanaka, Y. (1999) Embrittlement of austempered spheroidal graphite cast iron. *Int. J. Cast Met. Res.*, **11**, 539–544.
3 Komatsu, S, Osafune, Y., Tanaka, Y., Tanigawa, K, Shibutani, S and Kyogoku, H. (2003) Embrittlement characteristics of fracture toughness in ductile iron by contact with water. *Int. J. Cast Met. Res.*, **16**, 209–214.
4 Martínez, R. A., Boeri, R. E. and Sikora, J. A. (2000) Embrittlement of ADI caused by contact with water and other liquids. *Int. J. Cast Met. Res.*, **13**, 9–15.
5 Martínez, R. A., Simison, S. N., and Boeri R. E. (2002) Environmentally assisted embrittlement of ADI—current understanding, Book of 2002 World Conference on ADI. Louisville, *KY. USA*. **91–96**, 26–27.

6 Martínez, R. A., Simison, S. N. and Boeri, R. E. (2003) Environmentally assisted embrittlement of ADI by contact with liquids. *Int. J Cast Met. Res.*, **16**, 251–256
7 Daga, B., Martínez, R. A., Simison, S. and Boeri, R. E. (2003) *Evaluación de las Propiedades de Dureza y Fractomecánicas del ADI en Contacto con Agua*. *Annals of the Congress SAM/CONAMET/MATERIA Symposium*. San Carlos de Bariloche, Argentina, 647–650.
8 Zanotti, P., Simison, S. N., Martínez, R. A. and Boeri R. E. (2005) *Caracterización del Fenómeno de Fragilización de ADI en Contacto con Diferentes Medios Fluídos*. *Annals of the Binational Congress SAM/CONAMET 2005*, Mar del Plata, Argentina, pp. 37–43.
9 Masud, L., Martínez, R. A., Simison, S. and Boeri, R. E. (2003) Embrittlement of austempered ductile iron on contact with water—testing under applied potential. *J. Mat. Sci.*, **38**, 2971–2977
10 Caballero, L., Elices, M. and Parkins, R. N. (2005) Environment sensitive fracture of austempered ductile iron. *Corrosion*, **61**, 51–57.
11 Jones D. A. (1995) *Principles and Prevention of Corrosion*, 2nd edn. Macmillan Publ. Company, New York.
12 Hertzberg R. W. (1989) *Deformation and Fracture Mechanics of Engineering Materials*. 3rd edn. Wiley, Singapore.
13 Galvele, J. R. (1999) Past, present, and future of stress corrosion cracking. *Corrosion*., **8**, 723–731.
14 (1992) *ASM Handbook*, Vol. **13**, 9th edn., ASM International, OH, USA.
15 Shibutani, S. (2007) Private communication.
16 Lemme, T., Martínez, R. A., Simison, S. N. and Boeri, R. E. (2004) Caracterización de la iniciación de fisuras en ADI en contacto con medios fluidos, Conference Minutes SAM–CONAMET 2004, La Serena, Chile., 457–462.
17 Rivera, G. Boeri, R. and Sikora, J. (1995) Revealing the solidification structure of nodular iron, *Int. J. Cast Met.*, **8**, 1–5.
18 Boeri, R. and Weingberg, F. (1993) *Int. J. Cast. Met.*, **6**. 153–158
19 Rivera, G., Boeri, R. and Sikora, J. (1999) Influence of the solidification microstructure on the mechanical properties of ductile iron. *Int. J. Cast Met. Res.*, **11**, 533–538.
20 Laine, B., Simison, S. N., Martínez, R. A. and Boeri, R. E. (2002) Rol de la microestructura del ADI en el fenómeno de fregilización por contacto con agua, Annals of the Congress CONAMET/SAM–MATERIA Symposium, Santiago de Chile, Chile., 121–126.
21 Anderson, T. L. (1994) *Fracture Mechanics. Fundamentals and Applications*. CRC Press; Boca Raton, FL, USA.
22 Greno, G. L., Otegui, J. L., Boeri, R. E. (1999) Mechanisms of fatigue crack growth in austempered ductile iron. *Int J of Fatigue*, **21**, 35–43.
23 Boeri, R. E. and Martínez, R. A. (2013) Embrittlement of ADI by contact with liquids: influence of alloy content and preventive methods. *Mater. Sci. Technol.*, **29**, 665–671.
24 Martinez, R. A. (2010) Fracture surfaces and the associated failure mechanisms in ductile iron with different matrices and load bearing. *Engineering Fracture Mechanics.*, **77**, 2749–2762.
25 Lynch, S. (1988) Environmentally assisted cracking: overview of evidence for an adsorption-induced localized slip process. *Mater. Forum.*, **11**, 268–283.